Influence of Different Compensation Modes on Morphological and Electrical Characteristics of Secondary Arcs

Hongshun Liu, *Member*, *IEEE*, Zhiyuan Zhang, Tian Xia, Jingjing Yang, Qiuqin Sun, and Qingquan Li

***Abstract*—UHV transmission lines are usually equipped with high-voltage shunt reactors. These reactors and the resulting degree of compensation affect the voltage, current, and other electrical characteristics of secondary arcs. In this paper, a low-voltage experimental simulation setup to produce secondary arcs in different compensation modes is established, and the morphological and electrical characteristics of recorded arc images and discharge waveforms are analyzed. For morphological characteristics, the degree of secondary arcs is compared for different compensation modes. For electrical characteristics, the arc waveform, volt–current characteristics, and zero-current time of secondary arcs are compared for different compensation modes. These results provide a foundation to determine the time of extinction of secondary arcs on overhead lines in the case of compensation, as well as technical support to develop effective arc suppression and extinction techniques.**

***Index Terms*—Compensation mode, electrical characteristic, morphological characteristic, secondary arc.**

I. Introduction

FOR a single-phase grounding fault ultra-high voltage (UHV) transmission line, the non-fault phase continues the electromagnetic and electrostatic coupling power supply to the fault point by creating a secondary arc (SA) after eliminating the fault phase [1]–[3]. If this is not promptly extinguished, the circuit breaker closes and causes an arc grounding fault, which leads to a single-phase automatic reclosing failure [4]–[6]. UHV transmission lines are usually equipped with high-voltage shunt reactors, which not only provide parallel compensation but also restrain the SA. Regardless of the shunt reactor, the different degrees of compensation coupled with changes in the secondary arc current (SAC) and arc length lead to changes in the electrical characteristics, such as voltage and current [7]. UHV transmission lines extend over great distances under high operating voltages, making it more difficult to extinguish SAs than on general transmission lines [8], [9]. Thus, research into the arcing and extinction properties of SAs on UHV transmission lines is critical to develop successful arc suppression and extinction techniques.

Scholars conducted extensive SA simulation experiments and discovered some arc properties and laws, as well as the factors that influence arc extinction timing. An extensive experimental study was performed to investigate the motion characteristics of SAs, in which the effect of wind on the arc column was investigated in detail by analyzing the captured discharge images [10]. According to an experimental setting for simulating the action of SAs across an insulator string, the development of the volt-current characteristics of SAs has been systematically studied to represent the repeated mechanism of ignition and extinction [11]. The components and evolution of SAs were addressed, as well as an improved algorithm to solve the problems of discontinuous and false edges caused by conventional operators [12]. Based on field experiments, the voltage waveforms and arc extinction time were analyzed, and the correlations between recovery voltage, SAC and arc extinction time were examined [13]. However, the above studies did not consider the influence of the compensation mode on SAs, and there has been a lack of research on the characteristics of arcing, morphology, and arc root motion during SA movement under different compensation modes. In addition, many digital simulations on secondary arcs have been carried out based on secondary arc waveform data from experiments over past decades, but it is difficult to completely consider all the factors influencing SAs on the transmission line [14]–[16]. There is a need for appropriate simulations of the electrical, morphological, and extinction characteristics of SAs.

Physical experiments can analyze the physical mechanisms and macroscopic movement of SAs, but the strongly random behavior of such arcs means that many experiments are required. However, the limitations imposed by site conditions make it difficult to repeat field experiments multiple times, making simulations essential. To investigate changes in the morphological and electrical characteristics of SAs under

Manuscript received August 2, 2021; revised September 4, 2021; accepted October 14, 2021. Date of online publication August 18, 2022; date of current version December 31, 2023. This study is supported by the Shandong Natural Science Foundation Project (Grant No. ZR2020ME196) and the State Key Laboratory of Alternate Electrical Power System with Renewable Energy Sources (Grant No. LAPS2200).

H. S. Liu (corresponding author, email: lhs@sdu.edu.cn; ORCID: https://orcid.org/0000-0003-2103-2020), J. J. Yang and Q. Q. Li are with the School of Electrical Engineering, Shandong University, Jinan 250061, China.

Z. Y. Zhang is with the State Grid Jinan Power Supply Company, Jinan 250012, China.

T. Xia is with the State Grid Tianjin Chengdong Electric Power Supply Branch, Tianjin 300171, China.

Q. Q. Sun is with the College of Electrical and Information Engineering, Hunan University, Changsha 410082, China.

DOI: 10.17775/CSEEJPES.2021.05500

different compensation modes, the equivalent inductance of the shunt reactor is added to the original experimental simulation platform [11]. In this paper, simulations of SAs are performed for both under- and over-compensation conditions, and the electrical and morphological characteristics for different compensation modes are compared from the comprehensive perspectives of arc images, discharge waveforms, volt–ampere characteristics, and zero-current characteristics.

The remainder of this paper is organized as follows. Section II presents the experimental setup to simulate SAs under different compensation modes. Section III analyzes the influence of the compensation mode on the arcing degree through the binary processing of arc images. Section IV compares and analyzes the voltage and current waveforms of SAs under different compensation modes. Section V investigates the extinction characteristics of SAs and further analyzes the influence of the compensation mode on the zero-current time. Section VI presents the processed voltage and current data of SAs and discusses the volt–current characteristics under different compensation modes. Section VII compares and analyzes the arc extinction time, maximum potential current, and maximum recovery voltage of SAs under different compensation modes. Section VIII presents the conclusion.

II. Experimental Setup

A. Feasibility Analysis of Low Voltage Simulation Experiment

The SA belongs to the free combustion arc in the atmosphere, which is a capacitive long gap arc generated and developed in the gas medium produced by inductive short-circuit arc gasification. The extinction of the SA is related to the rising rate of the recovery voltage applied at both ends of the electrode and the air gap's dielectric strength recovery rate. Since the rising rate of recovery voltage is commonly related to transmission line structure and is easily restricted by line capacitive impedance, the simulation loop must be as simple as possible and easy to experiment with many times [3], [17], [18]. Much research has gone into the SA self-extinguishing simulation experiment. Considerable experiments performed by China Electric Power Research Institute (CEPRI) and Russian Siberia Research Institute of Power Engineering indicate that once the short-circuit current is in the range of 30–120 A, the arc extinction time does not change very much [19]–[21]. Even when the short-circuit current is greater than 1 kA, the arc extinction time changes very little, so the simulation experiment can use a small current instead of a UHV high voltage line [22]–[24].

Because the arc length of SAs is long and the arc characteristics of the arc column's internal and external parts are the same, the arc channel characteristics per unit length can be considered consistent, and the self-extinguishing time of SA is associated with the recovery voltage gradient but not directly related to the recovery voltage value. As a result, the SA with a length of l m in UHV lines can be approximately replaced by a low voltage short arc with a length of l/n m based on ensuring the equivalence of the recovery voltage gradient. The supply voltage is reduced to l/n in this case, and the line impedance is reduced by n times. Primarily, the inductance is reduced by n times, and the capacitance is increased by n times. Therefore, the laboratory short arc simulation under low voltage can investigate the long SA of UHV lines, and the experimental simulation is equivalent.

Previous research on the equivalent study of UHV SA using this low-voltage, low-current, short-gap SA simulation experimental platform yielded fruitful findings. It can be seen from the above analysis that by using a smaller arc current and a shorter arc gap in the experimental setup, it is possible to simulate UHV SA.

B. Topology of Main Circuit

This experiment was carried out at the High-Power Laboratory of CEPRI. The simplified experimental simulation circuit for a SA is shown in Fig. 1. Its main components are an AC power source (peak voltage of 11.6 kV), an equivalent capacitance C, a reactor L_0, a shunt compensation reactor L, circuit breakers CB_1, CB_2, and CB_3, an insulator string, and a fuse. The reactor and the capacitor branch produce short-circuit current and SA respectively. L simulates the equivalent inductance of the high-voltage shunt reactor on the transmission line, and the compensation mode is changed by varying the values of C and L. The equivalent capacitance C and effective values of SAC are expressed as follows:

$$C = (2C_1 + C_0/2)l \tag{1}$$

$$I = j\omega U_m C \tag{2}$$

where C_1 and C_0 represent the interphase capacitance and relative ground capacitance per unit length respectively, l represents the length of the overhead line, I represents the SAC in non-compensation, ω is the angular frequency, and U_m is peak voltage of power source.

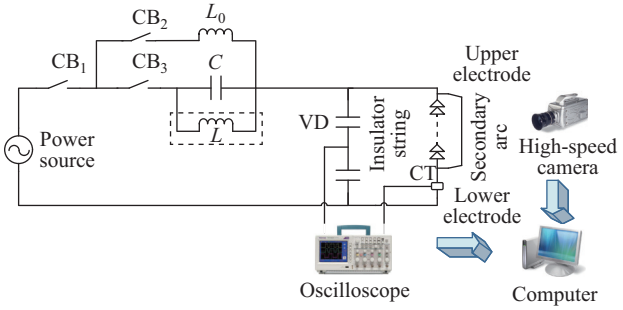

Fig. 1. Simplified experimental simulation circuit.

The function of the insulator string is to provide a certain recovery voltage gradient, so that the recovery voltage gradient of the simulated experimental arc channel is consistent with that of the SA channel in the actual line. In addition, the SA of UHV transmission lines often occurs near the insulator string, and the existence of the insulator string is helpful to better simulate the shape and motion of the SA close to the actual transmission line. In this paper, the suspended glass insulator is used in the insulator string, which has a total height of 68 cm. The two electrodes of the insulator string are connected by a Ni-Cr alloy wire to form an arc-striking channel by generating a short-circuit arc, and the electrode

spacing is 53 cm. The recovery voltage gradient is 21.9 kV/m (the peak supply voltage divided by the distance between the upper and lower electrodes of the insulator string).

The operating sequence of the switch in the experiment is as follows. First, CB_3 is turned on, and CB_2 and CB_1 are closed to simulate the inductive short-circuit current of 1 kA in the UHV line, the reactor L_0 is set as 36.88 mH. Then, CB_3 is closed and CB_2 is turned on to simulate the SA of the UHV line under different compensation modes. The voltage and current of the arc are obtained with a 1000:1 voltage divider (VD) and a current transformer (CT), respectively. In this paper, a high-speed camera (Motion Pro X3) based on a charge coupled device (CCD) sensor is used as the observation equipment, the maximum image resolution is 1280 × 1024, the frame rate is 500 fps, the minimum exposure time is 1 μs, and the longest shooting time is 6.5 s. Based on the length of the SA, the focal length of the lens is set to 80 mm and the lens aperture is set to 1.4.

The relevant parameters of the experimental setup are shown in Table I, which are used to generate SAC of different natures with an amplitude of 30 A in the three compensation modes. The reactor L and equivalent capacitance C can be calculated by (3) and (4) for the under- and over-compensated cases, respectively.

$$I_C = \frac{U_m}{X_C} - \frac{U_m}{X_L} = U_m\omega C - \frac{U_m}{\omega L} \tag{3}$$

$$I_L = \frac{U_m}{X_L} - \frac{U_m}{X_C} = \frac{U_m}{\omega L} - U_m\omega C \tag{4}$$

where I_C and I_L represent the SAC for under- and over-compensation, respectively.

TABLE I
PARAMETERS OF EXPERIMENTAL SETUP

Compensation mode	Current property	L (H)	C (μF)
Non-compensation	Purely capacitive	0	8
Under-compensation	Capacitive compensation	1.2	16
Over-compensation	Inductive compensation	0.6	8

III. INFLUENCE OF DIFFERENT COMPENSATION MODES ON ARCING DEGREE

To observe the influence of the compensation mode on the arcing degree for the SA, arc images for three compensation modes at the same time under the same conditions (SAC of 30 A, recovery voltage gradient of 21.9 kV/m, and sampling period of 0.002 s) are selected for analysis, as shown in Fig. 2. Among the three groups of images, the arcing degree of the SA is the most intense in the non-compensation case. At 0.1 s, the arc is dissipated in the under- and over-compensation cases, while it still burns in the non-compensation case.

An SA is an air arc in a long gap and exhibits complex behavior as affected by wind, electromagnetic, and thermal buoyancy forces, as well as other factors. Its morphological characteristics are subject to instability and exhibit strongly random behaviors. Therefore, accurate conclusions cannot be obtained by relying solely on qualitative analyses and comparisons of typical images. To determine the common characteristics of SAs, images of the initial stage of SA for three compensation modes are processed using the Color Threshold Limiter toolbox in the MATLAB software to give binary images, as shown in Fig. 3. The pixel area (AREA) of each arc image is obtained using the Image Region Analyzer toolbox to process the binary images. Then, averaging three groups of AREA values at the same time for each compensation mode provides the influence of the arcing area for different compensation modes during the short-circuit arc stage, as shown in Fig. 4. The burning intensity of the arc varies periodically, with the arcing area reaching a maximum at the time of peak voltage before decreasing gradually and

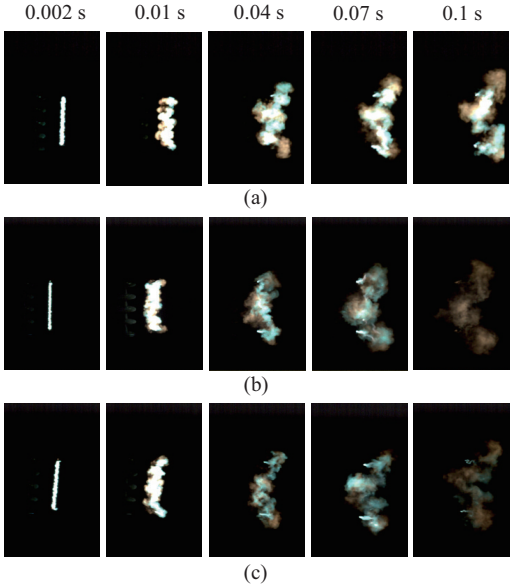

Fig. 2. Images of SAs for different compensation modes: (a) Non-compensation, (b) under-compensation, and (c) over-compensation.

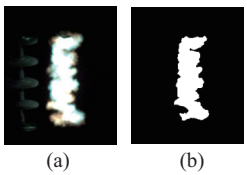

Fig. 3. Binary processing of short-circuit arc: (a) Before processing and (b) after processing.

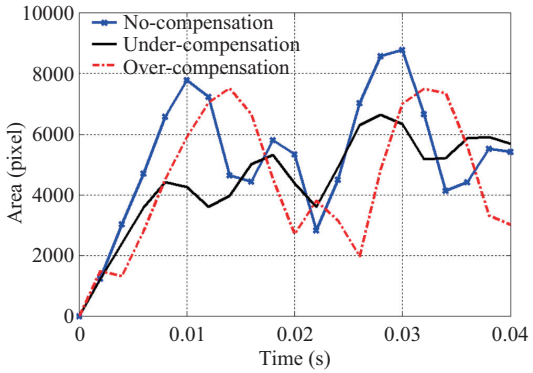

Fig. 4. Comparison of the arcing area for the short-circuit arc for different compensation modes.

again reaching a maximum at the next voltage peak. From 0 to 0.04 s, the maximum arcing area of the SA for the non-compensation mode is more than 8000 pixels, and its arcing degree is the most intense, which is consistent with the images in Fig. 2.

IV. Waveform Analysis of SAs for Different Compensation Modes

This section analyzes the influence of the compensation mode on the electrical characteristics of SAs for the same arc current (30 A) based on typical measured experimentally arc current and voltage waveforms. The discharge characteristics and recovery voltage characteristics of the SAC under three compensation modes are shown in Table II, and the following parts are analyzed in detail respectively.

A. Waveforms of the SA for Non-compensation

When $C = 8$ μF in the experimental circuit of Fig. 1 and L is not installed, the current in the branch that produces the SA is purely capacitive, which is the non-compensation mode, and the SAC is 30 A. From the current waveform in Fig. 5(a), stage 1 (0.1–0.19 s) is the current short-circuit stage with an alternating short-circuit current and a maximum amplitude of approximately 1 kA. Stage 2 (0.19–0.63 s) is the secondary arc stage with a maintenance time of about 0.44 s, in which the maximum current amplitude is 310 A, and a total of 44 strong breakdown discharges occurred (primarily in the form of electrical breakdown). The voltage waveform in Fig. 5(b) indicates that the arc voltage is square with an amplitude of about 1.5 kV in the short-circuit arc stage (stage 1). The maximum release voltage is 14.12 kV during the secondary arc stage (stage 2), and a relatively stable recovery voltage is formed at the end of the SA discharge at 0.63 s with a maximum recovery voltage of 26.93 kV. We performed Fourier analysis on the current and voltage of the SA, which has the largest proportion of the power frequency component and also contains odd harmonic components such as the third and fifth harmonics. The amplitude of the harmonic component gradually decreases with the increase of the number of times, and the current and voltage components of the power frequency are 28 A and 3.12 kV respectively.

B. Waveforms of SA for Under-compensation

When $L = 1.2$ H and $C = 16$ μF in the experimental circuit, the current in the branch that produces the SA is capacitive and under the under-compensation mode. The SAC is 30 A. From the current waveform of Fig. 6(a), stage 1 (0.1–0.2 s) consists of a short-circuit stage and has an alternating current with a maximum amplitude of approximately 1 kA. The current waveform is shown in Fig. 6(a). Stage 2 (0.2–0.28 s) is the secondary arc stage, with a maintenance time of approximately 0.08 s. During this period, the maximum amplitude of the arc discharge current is 118.7 A, and a total of eight electric breakdown discharges occurred. The voltage waveform in Fig. 6(b) shows that the short-circuit arc stage (stage 1) has a square wave arc voltage with an amplitude of 1.2–1.5 kV. In the secondary arc stage (stage 2), the maximum discharge voltage reaches 6.25 kV. The discharge ends after 0.28 s, and a recovery voltage with beat frequency characteristics is produced at the upper and lower ends of the electrode. The beat periodicity is 4 and the maximum recovery voltage is 28.75 kV. The current has the largest proportion of the power frequency component of 27.26 A and contains a relatively more complex higher harmonic component than the non-compensation. The power frequency component, the second harmonic, and the fourth harmonic component of the voltage make up the major part, corresponding to amplitudes of 2.89 kV, 1.32 kV, 0.86 kV, respectively.

TABLE II
Statistics of Discharge Information of SA for the Various Compensation Modes

Compensation mode	Secondary arc stage (Stage 2)				Max recovery voltage (kV)
	Max arc current (A)	Max arc voltage (kV)	Maintenance time (s)	Number of breakdowns	
Non-compensation	310	14.12	0.44	44	26.93
Under-compensation	118.7	6.25	0.08	8	28.75
Over-compensation	252.8	13.65	0.03	4	28.43

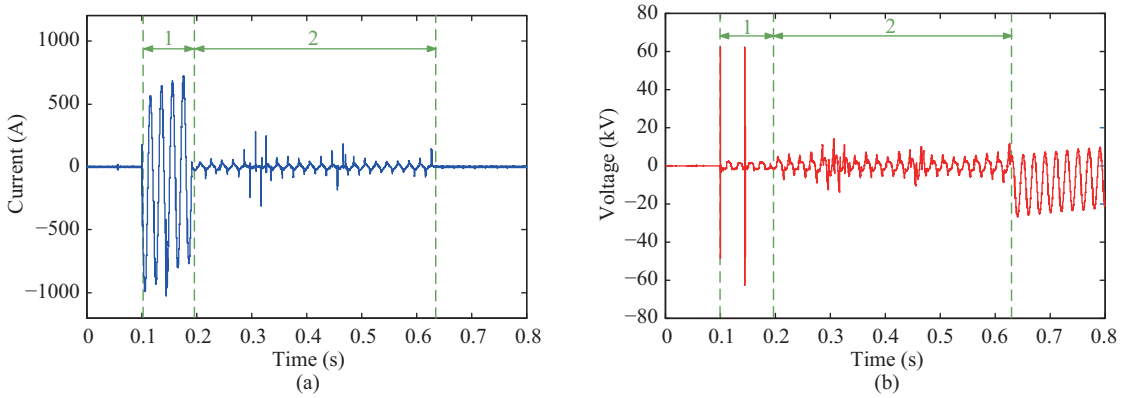

Fig. 5. Waveforms of the SA for non-compensation: (a) Current and (b) voltage.

In the case of compensation, the arc gap recovery voltage shows beat frequency characteristics, because the shunt reactor resonates with the interphase capacitor when installed on the line. After the SA goes out, the discharge circuit produces a resonant-free oscillation. At the same time, the arc voltage is the superposition of the interphase coupling voltage component and the free-oscillation component of the discharge circuit after disconnection of the normal phase; thus, the arc gap voltage has beat frequency characteristics. The free-oscillation component of the resonant circuit gradually decreases to 0, and there remains only the recovery voltage component of the interphase coupling voltage at both ends of the arc gap.

C. Waveforms of the SA for Over-compensation

When $L = 0.6$ H and $C = 8$ μF in the experimental circuit, the current in the branch that produces the SA is inductive, which is the over-compensation mode with a SAC of 30 A. The current waveforms in Fig. 7(a) indicate that stage 1 (0.1–0.21 s) is the short-circuit current stage, which is alternating with a maximum amplitude of 600 A. Stage 2 (0.21–0.25 s) is the secondary arc stage with a maintenance time of about 0.03 s where the maximum amplitude of the arc discharge current is 252.8 A, and a total of four electric breakdown discharges occurred. The voltage waveform in Fig. 7(b) indicates that the arc voltage is a square wave with an amplitude of 1–2 kV at the short-circuit arc stage (stage 1). The maximum discharge voltage reaches 13.65 kV in the secondary arc stage (stage 2), and the arc discharge ends after 0.25 s. Similar to the under-compensation case, there is an arc gap recovery voltage with beat frequency characteristics between the two ends of the electrode with a beat periodicity of 3 and maximum recovery voltage of 28.43 kV. Thus, the maximum recovery voltage of the SA in the over-compensation case is close to that of the under-compensation case. The current and voltage have the largest proportion of power frequency components of 26.72 A and 2.95 kV, and contain more complex higher harmonic components. The voltage also contains a higher number of secondary and third harmonics of 0.67 kV and 0.84 kV.

V. Analysis of Zero-current Time of SAs for Different Compensation Modes

To further analyze the details of waveforms during SAs, a power frequency of 50 Hz is selected and amplified in the secondary arc stage. The waveforms for the three different compensation modes are shown in Fig. 8.

During the motion of SA, although the arc channel is constantly exchanging energy with the surrounding space to ensure the arc resistance has a strong nonlinearity, the arc resistance is still resistive, which causes the zero-crossing points of the voltage and current waveforms to occur at the same time. Due to the thermal inertia of the SA, the peak current usually lags behind the peak voltage by 1–3 ms. The SAC is relatively small, the waveform distortion is severe, and the voltage waveform is saddle-shaped. The nonlinear behavior of the arc is characterized by the generation of high-frequency components and distortion in the voltage waveform with two

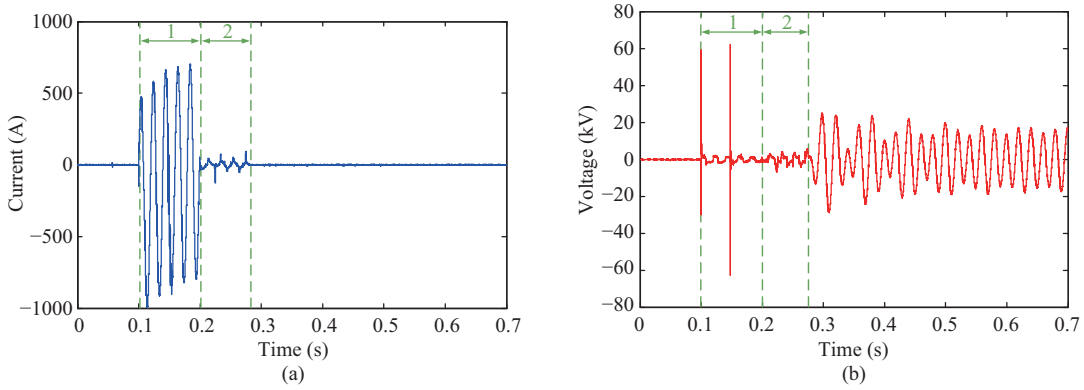

Fig. 6. Waveform of the SA in under-compensation: (a) Current and (b) voltage.

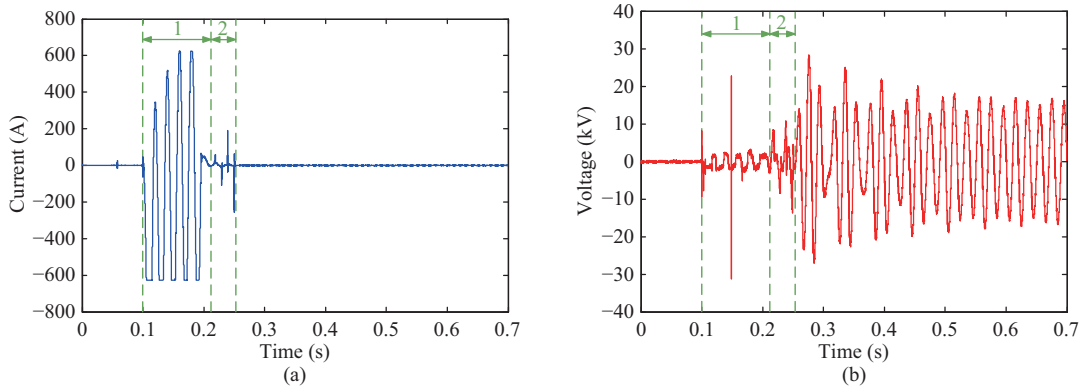

Fig. 7. Waveforms of the SA in over-compensation: (a) Current and (b) voltage.

peaks in each half-period. The peak value of the arc voltage in each cycle in the under-compensation case is quite different and exhibits strong instability. One of the main causes of this is the dynamic change of the arc length as a result of interactions between various electrical, thermal buoyancy, and wind forces.

As indicated by the green arrows in Fig. 8(a), when the voltage crosses zero, there is a transient recovery voltage with a large amplitude, high frequency, and short influence period. When the current crosses zero, it remains zero for some time. This latter zero-current phenomenon is because the arc temperature decreases faster in the zero-crossing stage of the current during the burning of the SA and is not high enough to maintain thermal dissociation of particles in the arc column. Thus, the deionization process controls the movement of the particles. Several electrons combine with neutral particles, which combine with positive ions to form new neutral particles. The neutral particles cannot form a conductive channel, and the zero-current phenomenon arises.

The zero-current time has a notable influence on the arc extinction. With an increased zero-current time, the time at which the arc input power is zero also increases. After the zero-crossing stage, a decreased temperature causes the arc column to be relatively thin and easier to extinguish. As the zero-current time significantly affects extinction of the SA, it is necessary to analyze the influence of the compensation mode on the zero-current time. Fig. 9 shows typical arc current waveforms and their zero-current stages for the different compensation modes.

By assuming that data points with currents less than 1 A correspond to the zero-current phenomenon, it is possible to obtain the duration of each zero-current stage for the compensation modes, as shown in Table III. The average zero-current time is the shortest for the non-compensation mode,

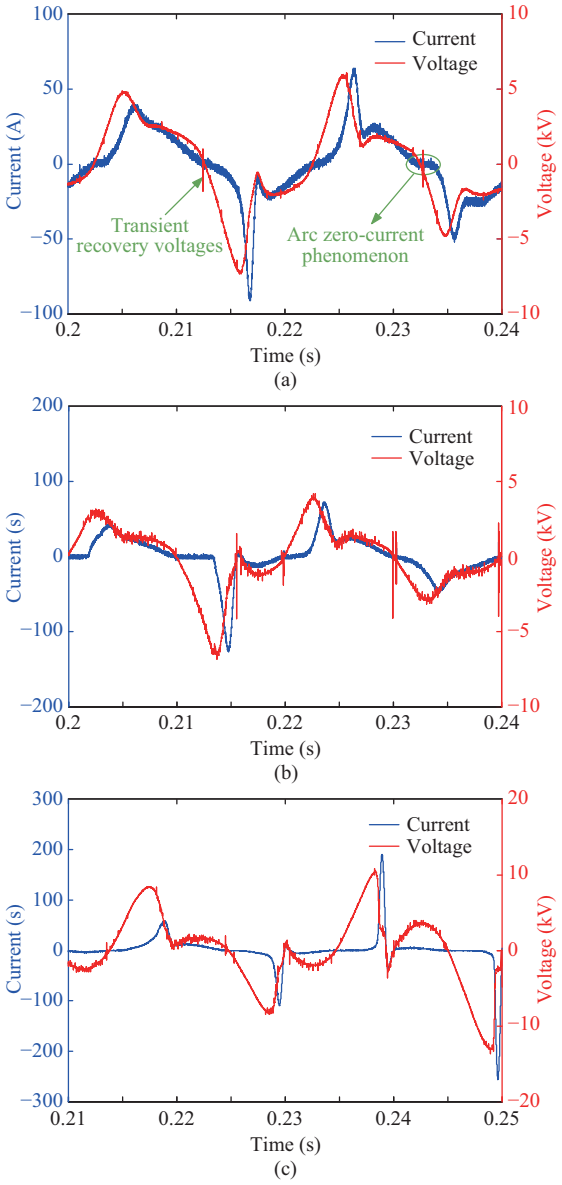

Fig. 8. Two-cycle waveform amplification of secondary arc stage for different compensation modes: (a) Non-compensation, (b) under-compensation, and (c) over-compensation.

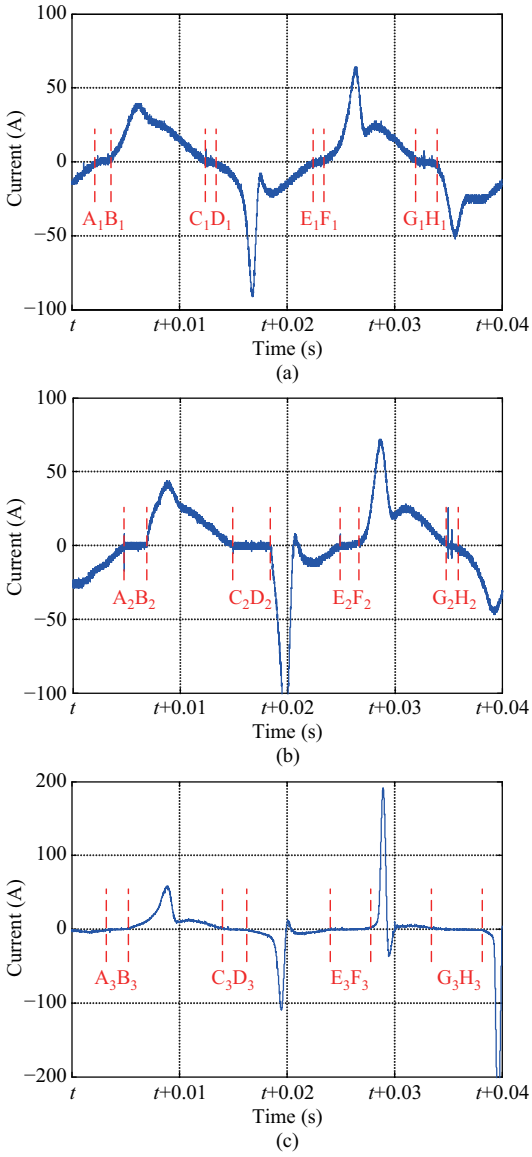

Fig. 9. Current waveforms in the zero-current stage of SAs for different compensation modes: (a) No-compensation, (b) under-compensation, and (c) over-compensation.

TABLE III
STATISTICS OF THE ZERO-CURRENT TIME FOR THE VARIOUS COMPENSATION MODES

Compensation mode	Duration of zero-current stage (s)				Average zero-current time (s)	Arc duration (s)
	AB	CD	EF	GH		
Non-compensation	0.00139	0.00141	0.00155	0.00217	0.0016	0.44
Under-compensation	0.00219	0.00353	0.00208	0.00109	0.0022	0.08
Over-compensation	0.00229	0.00232	0.00411	0.00448	0.0033	0.03

is intermediate for the under-compensation mode, and is the longest for the over-compensation mode. The results of the corresponding arcing time for the SA show that it is the longest for the no-compensation mode, is intermediate for the under-compensation mode, and is the shortest for the over-compensation mode. This proves that the arc column is more easily extinguished with an increasing zero-current time.

VI. ANALYSIS OF VOLT–CURRENT CHARACTERISTICS OF SAS FOR DIFFERENT COMPENSATION MODES

A. Volt–current Characteristics of the Typical SA

The current and voltage waveforms of a typical SA in one cycle (0.02 s) are shown in Fig. 10. The morphology of a SA is related to the heat exchange between the arc and atmospheric air. Moreover, the vol–current properties are closely related to arc burn stability, such as arc reignition. As the SA has an alternating current with a long gap, the current changes regularly and crosses zero twice over a specific time. If the arc current goes through zero, the arc gap's input energy is zero, the temperature decreases, and the arc naturally goes out. The SA can be reactivated with increasing voltage and current supplies. Thus, the burning of the second arc is a repeated re-burning and extinction process, which can also be seen in the volt-current characteristics.

Figure 11 shows the volt–current characteristics of the arc corresponding to Fig. 10. Fig. 11 shows that the shape of the waveform is nearly symmetric about the origin, which is similar to a hysteresis loop. This is because the material and layout of the upper and lower electrodes are the same. The line segments O–A–B–O and O–C–D–O correspond respectively to the positive and negative waveforms in Fig. 9. The line segment O–A indicates that the arc voltage increases rapidly after the current crosses zero. When the breakdown voltage (point A) is reached, the voltage decreases and the current increases. When the SAC reaches its maximum (point B), the current and voltage gradually drop to zero, and the arc goes out naturally. In segment A–B–O, the particles in the parallel gap collide with each other due to thermal motion at high temperatures, the number of charged particles varies over time, and the conductance of the arc first increases before decreasing. The process in the red oval in Fig. 11 shows that when the voltage drops to a certain level, it increases slightly to maintain arc burning.

B. Volt–current Characteristics for Different Compensation Modes

To analyze the influence of the compensation mode on the volt–current characteristics of a SA, the voltage and current

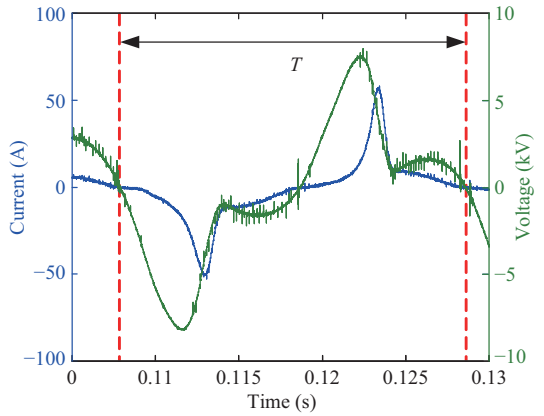

Fig. 10. Current and voltage waveforms of a typical SA.

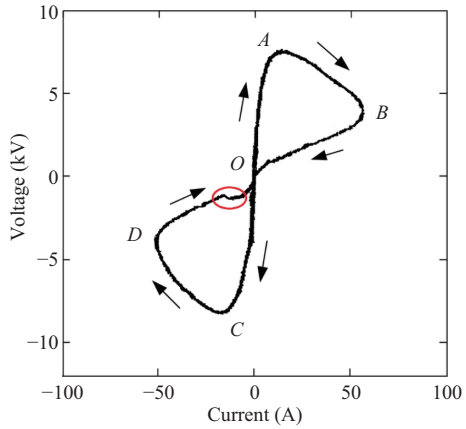

Fig. 11. Volt–current characteristics of a typical SA.

data of typical SAs for the three compensation modes are processed. As shown in Figs. 12–14, the curves are approximately centrally symmetric with a fan-shaped loop. The breadth of the volt-current characteristic curve is small in the secondary arc stage. However, as the arcing time increases, the breakdown voltage grows, and the area within the closed curve expands. This indicates that the discharge power rises gradually, and the arc discharge becomes more severe. In the later arcing stages, the area enclosed by the volt–current characteristic curve expands rapidly and becomes closer to a triangle shape. In the increasing recovery voltage stage, the volt–current characteristic curve is a rising curve with a large slope and becomes nearly parallel to the vertical axis. When the recovery voltage reaches breakdown, the arc quickly breaks down the electrode gap. With the continuous burning and extinction of the arc, the combined action of the electrical, thermal buoyancy, and air resistance forces causes the arc length to grow continuously,

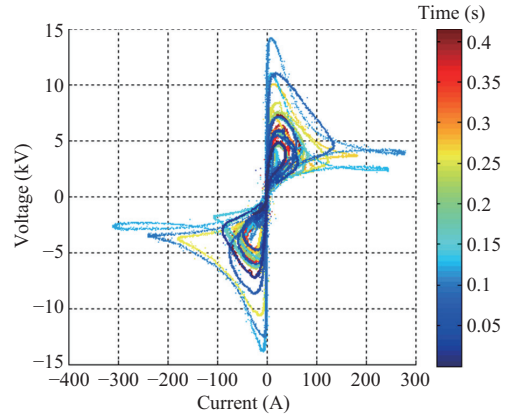

Fig. 12. Volt–current characteristics of SA for non-compensation.

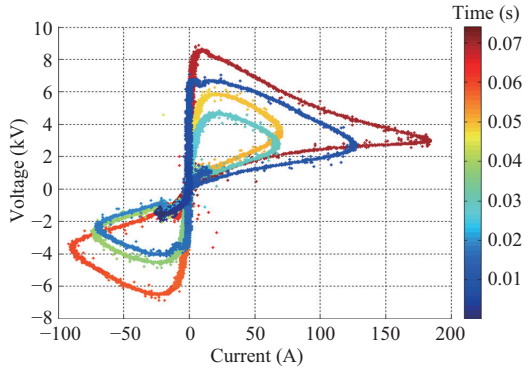

Fig. 13. Volt–current characteristics of the SA for under-compensation.

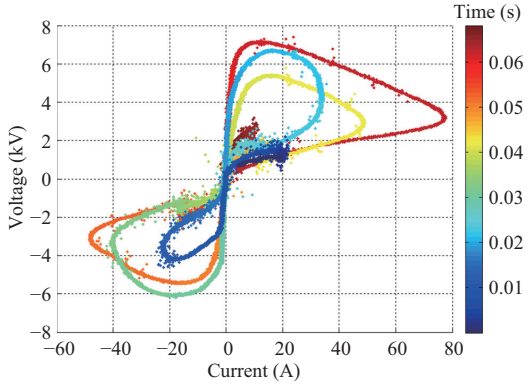

Fig. 14. Volt–current characteristics of the SA for over-compensation.

and the arc gap breakdown voltage increases. Finally, at the zero-current time of the secondary current, the voltage and current decrease, and the arc goes out.

From Fig. 12, the breakdown of the SA occurs more than 20 times in the non-compensation mode, and the SAC and breakdown voltage increase gradually with increasing reignitions. The maximum breakdown voltage is close to 15 kV, and the absolute value of the maximum secondary current is more than 300 A. The area surrounded by the volt-current characteristic curve corresponding to the breakdown of the SA gradually increases, indicating a large power of the discharge and intensely burning arc, which does not lead to its extinction.

In the case of under-compensation, Fig. 13 shows that reignition of the SA occurs seven times with a maximum breakdown voltage of 8 kV and a maximum potential current less than 200 A. Thus, SA burning in the under-compensation mode is not as intense as in the non-compensation mode, and there are fewer reignitions. Fig. 14 shows that the behavior of the SA in the case of over-compensation is similar to that for under-compensation with a low number of reignitions (six), a maximum breakdown voltage less than 8 kV, a maximum SAC less than 80 A, and an arc burning intensity less than for the non-compensation mode.

VII. Analysis of the Influence of Compensation Mode on Electrical Characteristics of SAs

The waveforms of the SA obtained from the low-voltage simulation experiments illustrate three characteristic electrical parameters: extinction time, maximum SAC, and maximum recovery voltage. These parameters can be used to characterize the intensity of the arc discharge, discharge time, and recovery voltage of the arc gap. Ten groups of experimental data on SAs in the three compensation modes under the same conditions are selected and compared. The influences of the compensation mode on the arc extinction time, maximum SAC, and maximum recovery voltage after arc extinction are examined, as shown in Fig. 15.

From Figs. 15(a) and (b), the SA is successfully ignited nine times in the non-compensation mode for the same SAC, five times in the under-compensation mode, but only once in the over-compensation mode. Therefore, in the absence of successful arc ignition, there is no arc extinction time or secondary arc current, and Fig. 15(a) and (b) have several missing values. Fig. 15(a) shows that there are some differences in the arc extinction times between the compensation modes. In the case of non-compensation, the arc duration is mostly from 0.07–0.09 s, with the shortest being 0.0572 s and the longest 0.1363 s without deviating greatly from its average. For under-compensation, the arc duration is mostly concentrated from 0.07–0.12 s with the shortest being 0.0161 s and longest 0.1784 s, but it fluctuates considerably. For over-compensation, the possibility of arcing is relatively low, and only one arc occurs with a duration of 0.0371 s. The average arc extinction time is calculated as 0.095 s in the non-compensation mode, 0.098 s in the under-compensation mode, and 0.0371 s in the over-compensation mode (calculations are performed only for experimental data on successful arc ignitions). The experimental results indicate that the rate of successful ignition of SAs in the over-compensation mode is low and the arc duration is short.

The maximum SAC varies significantly between the three compensation modes, as shown in Fig. 15(b). In the non-compensation mode, it does not deviate greatly from its average, but the under-compensation mode undergoes significant fluctuations. The average maximum SAC is calculated as 248.96 A in the non-compensation mode, 426.80 A in the under-compensation mode, and 131.33 A in the over-compensation mode. The SA is a strong discharge, and the measured values of the current fluctuate, making it difficult to draw accurate conclusions. However, data obtained in the

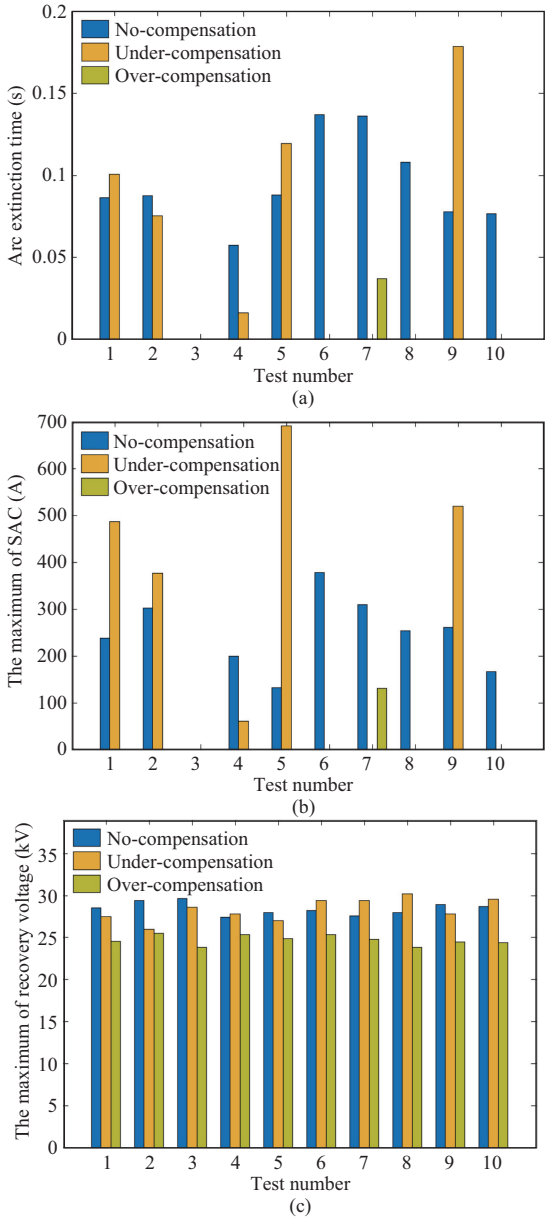

Fig. 15. Electrical characteristics of SAs in the different compensation modes: (a) Arc extinction time, (b) Maximum SAC, and (c) Maximum recovery voltage.

experiments show that the average of the maximum SAC has a decreasing trend in the order of under-compensation, non-compensation, and over-compensation.

Figure 15(c) illustrates the influence of different compensation modes on the maximum recovery voltage after arc extinction. The maximum recovery voltages in the non-compensation and under-compensation modes are similar, but the values in the over-compensation mode are much lower. The calculated average maximum recovery voltage after arc extinction is 28.44 kV in non-compensation, 28.40 kV in under-compensation, and 24.70 kV in over-compensation.

VIII. Conclusion

An equivalent inductance corresponding to a parallel reactor was installed in a SA experimental simulation circuit. Comparative experiments simulating SAs were performed for non-compensation, under-compensation, and over-compensation modes. The results of this paper can provide a theoretical basis and technical support for the further study of arc suppression and extinction of UHV transmission lines. The following conclusions are drawn from the experimental results:

1) Under the same conditions, the arcing degree in the non-compensation mode is the most intense. The arcing degree and characteristics of the SA are affected by the wind, electromagnetic, and thermal buoyancy forces, as well as other factors. The intensity of arc burning varies periodically, and the arc area reaches a maximum at the peak voltage.

2) From the voltage and current waveforms of the SA, the recovery voltage exhibits the characteristics of a sinusoidal beat wave for the non-compensation and over-compensation modes after SA extinction.

3) The average zero-current time is the shortest for the non-compensation mode, is intermediate for the under-compensation mode, and is the longest for the over-compensation mode. The longer the zero-current time, the longer it takes for the arc input power to become zero. After the zero-crossing stage, the arc column is more likely to be extinguished with a decreasing temperature.

4) Analysis of the volt–current characteristics of five groups of SAs under three different compensation modes shows that the compensation mode affects the SA burning characteristics and reignition times. In the under-compensation and over-compensation modes, the reignition times and discharge power of the SA are reduced. The SA in the non-compensation mode is the most difficult to extinguish.

5) The probability of successful arc ignition decreases in turn for the non-compensation, under-compensation, and over-compensation modes. For the over-compensation mode, the success rate of arc ignition is low and the arc duration is short. For the non-compensation mode, the maximum SAC does not deviate greatly from its average value. Whereas the under-compensation mode undergoes significant fluctuations. The maximum recovery voltage for the over-compensation mode is lower than that for the non-compensation and under-compensation modes.

References

[1] W. Shi, F. Li, Y. H. Han, and Y. G. Li, "The effect of ground resistance on secondary arc current on an EHV transmission line," *IEEE Transactions on Power Delivery*, vol. 20, no. 2, pp. 1502–1506, Apr. 2005.

[2] Members of the IEEE Power System Relaying Committee working Group, "Single phase tripping and auto reclosing of transmission lines-IEEE Committee Report," *IEEE Transactions on Power Delivery*, vol. 7, no. 1, pp. 182–192, Jan. 1992.

[3] Y. Goda, S. Matsuda, T. Inabe, and Y. Ozaki, "Insulation recovery characteristics after fault arc interruption on UHV (1000 kV Class) transmission lines," *IEEE Transactions on Power Delivery*, vol. 8, no. 4, pp. 1907–1913, Oct. 1993.

[4] I. M. Dudurych, T. J. Gallagher, and E. Rosolowski, "Arc effect on single-phase reclosing time of a UHV power transmission line," *IEEE Transactions on Power Delivery*, vol. 19, no. 2, pp. 854–860, Apr. 2004.

[5] O. Dias, F. Magrin, and M. C. Tavares, "Comparison of secondary arcs for reclosing applications," *IEEE Transactions on Dielectrics and Electrical Insulation*, vol. 24, no. 3, pp. 1592–1599, Jun. 2017.

[6] W. Wang, X. J. Zeng, L. J. Yan, X. Y. Xu, and J. M. Guerrero, "Principle and control design of active ground-fault arc suppression device for

full compensation of ground current," *IEEE Transactions on Industrial Electronics*, vol. 64, no. 6, pp. 4561–4570, Jun. 2017.
[7] M. R. D. Zadeh, M. Sanaye-Pasand, and A. Kadivar, "Investigation of neutral reactor performance in reducing secondary arc current," *IEEE Transactions on Power Delivery*, vol. 23, no. 4, pp. 2472–2479, Oct. 2008.
[8] H. S. Liu, J. J. Yang, L. Ji, Z. Wang, Z. N. Huang, X. S. Yang, and J. T. Wang, "Influence of hybrid reactive power compensation on the secondary arc of ultra-high-voltage transmission lines (May 2018)," *IEEE Access*, vol. 6, pp. 38115–38123, Jun. 2018.
[9] J. Schindler, C. Romeis, and J. Jaeger, "Secondary arc current during DC auto reclosing in multisectional AC/DC hybrid lines," *IEEE Transactions on Power Delivery*, vol. 33, no. 1, pp. 489–496, Feb. 2018.
[10] Q. M. Li, H. X. Cong, Q. Q. Sun, J. Y. Xing, and Q. Chen, "Characteristics of secondary AC arc column motion near power transmission-line insulator string," *IEEE Transactions on Power Delivery*, vol. 29, no. 5, pp. 2324–2331, Oct. 2014.
[11] H. S. Liu, R. C. Li, D. X. He, J. C. Wei, and Q. Q. Li, "Experimental study of multiple-reignition features of secondary arcs on EHV/UHV transmission lines," *IEEE Transactions on Industrial Electronics*, vol. 66, no. 4, pp. 3247–3255, Apr. 2019.
[12] Q. Q. Sun, F. W. Liang, F. Wang, H. X. Cong, Q. M. Li, and J. D. Yan, "Investigation on the geometrical characteristics of secondary Arc by image edge detection," *IEEE Transactions on Plasma Science*, vol. 46, no. 6, pp. 2016–2025, Jun. 2018.
[13] T. Tsuboi, J. Takami, S. Okabe, K. Aoki, and Y. Yamagata, "Study on a field data of secondary arc extinction time for large-sized transmission lines," *IEEE Transactions on Dielectrics and Electrical Insulation*, vol. 20, no. 6, pp. 2277–2286, Dec. 2013.
[14] Q. Y. Ma, B. Zheng, L. G. Ban, and Z. T. Xiang, "Secondary arc current analysis of an untransposed EHV/UHV transmission line with controllable unbalanced shunt reactor," *IEEE Transactions on Power Delivery*, vol. 30, no. 3, pp. 1458–1466, Jun. 2015.
[15] H. X. Cong, Q. M. Li, J. Y. Xing, and W. H. Siew, "Modeling study of the secondary arc with stochastic initial positions caused by the primary Arc," *IEEE Transactions on Plasma Science*, vol. 43, no. 6, pp. 2046–2053, Jun. 2015.
[16] X. Zhang, Z. Y. Xu, B. Gao, X. R. Xie, and K. Wang, "Compensation scheme for secondary arc current on four-circuit parallel transmission lines," *IET Generation, Transmission & Distribution*, vol. 10, no. 9, pp. 2079–2086, Jun. 2016.
[17] A. I. Megahed, H. M. Jabr, F. M. Abouelenin, and M. A. Elbakry, "Arc characteristics and a single-pole auto-reclosure scheme for Alexandria HV transmission system," *Electric Power Systems Research*, vol. 76, no. 8, pp. 663–670, May. 2006.
[18] L. Prikler, M. Kizilcay, G. Bán, and P. Handl, "Improved secondary arc models based on identification of arc parameters from staged fault test records," in *Proceedings of the 14th Power System Computation Conference (PSCC)*, Sevilla, Spain, 2002, pp. 1–6.
[19] Y. M. He, W. Li, K. Yang, B. Y. Cui, P. F. Zhang, R. J. Cao, J. M. Lin, and Y. C. Yuan, "The experimental research of secondary arc in 1000kV UHV systems in China," in *Proceedings of 2015 3rd International Conference on Electric Power Equipment-Switching Technology (ICEPE-ST)*, 2015, pp. 161–165.
[20] J. Y. Xing, Q. M. Li, H. X. Cong, J. S. Li, Q. Chen, and Q. Y. Li, "Physical mechanism and simulation method of the arc root jumping and arc length variation of the secondary arcs with long-distance transmission lines," *Transactions of China Electrotechnical Society*, vol. 31, no. 12, pp. 90–98, Jun. 2016.
[21] J. Q. Ran, Q. Yang, L. W. He, H. W. Liu, T. Zhou, and S. Y. Wei, "Improved mathematical model for single-ground arcing fault in medium voltage distribution networks," *CSEE Journal of Power and Energy Systems*, doi: 10.17775/CSEEJPES.2021.05120.
[22] M. C. Tavares, and C. M. Portela, "Transmission system parameters optimization-sensitivity analysis of secondary arc current and recovery voltage," *IEEE Transactions on Power Delivery*, vol. 19, no. 3, pp. 1464–1471, Jul. 2004.
[23] A. Carrus, F. M. Gatta, and E. Cinieri, "Secondary arc current interruption in an unconventional MV distribution system: digital simulation and experimental test results," in *Proceedings of the 3rd International Conference on Properties and Applications of Dielectric Materials*, Tokyo, Japan, 1991.
[24] Y. Z. Zhang, S. X. Xiu, Q. Tang, S. L. Jia, B. Chu, W. X. Mo, Y. Wang, and H. B. Su, "Interruption characteristics of high-speed switch in 500 kV fault current limiter with high coupled split reactance," *CSEE Journal of Power and Energy Systems*, vol. 9, no. 4, pp. 1577–1584, Jul. 2023.

Hongshun Liu received B.Sc. and Ph.D. degrees in Electrical Engineering from Shandong University, Jinan, China, in 2004 and 2010, respectively. Currently, he is an Associate Professor in Electrical Engineering at Shandong University, Shandong, China. His research interests include the modeling and simulation for power system electromagnetic transient processes, overvoltage and insulation coordination, arc discharge theory and its application (secondary arc and switching arc in UHV power system), etc.

Zhiyuan Zhang received a B.Sc. degree from China University of Mining and Technology, Xuzhou, China, in 2019, and an M.Sc. degree in Electrical Engineering from Shandong University, Jinan, China, in 2022. He is currently with the State Grid Jinan Power Supply Company, Jinan City, China. His research interests include secondary arc in UHV power systems and simulation for power system electromagnetic transient processes.

Tian Xia received B.Sc. and M.Sc. degrees from Shandong University, Jinan, China, in 2017 and 2020, respectively. She is currently with the State Grid Tianjin Chengdong Electric Power Supply Branch, Tianjin City, China. Her research interests include secondary arc discharge theory and its application in UHV power systems.

Jingjing Yang received a B.Sc. degree from the Shandong University of Science and Technology, Jinan, China, in 2017, and an M.Sc. degree in Electrical Engineering from Shandong University, Jinan, China, in 2020. She is currently pursuing a Ph.D. degree at Shandong University, Jinan, China. Her current research interests include the partial discharge of oil-pressboard insulation.

Qiuqin Sun received a B.Sc. degree from Chongqing University, Chongqing, China, and a Ph.D. degree from Shandong University, Jinan, China, in 2006 and 2012, respectively. He is currently a Professor with the College of Electrical and Information Engineering, Hunan University, Changsha, China. His research interests include electric arcs and electromagnetic transients in power systems.

Qingquan Li received a Ph.D. degree in Electrical Engineering from Xi'an Jiaotong University, Xi'an, China, in 2003. Currently, he is a Professor at Shandong University, Jinan, China. His research interests include lightning protection and grounding technology, high voltage insulation and measurement technology, and detection and diagnosis techniques for electrical equipment.